Monte Carlo simulation of the semimetal-insulator phase transition in monolayer graphene

Wes Armour,[1] Simon Hands,[2] and Costas Strouthos[3]
[1]*Diamond Light Source, Harwell Campus, Didcot, Oxfordshire OX11 0DE, United Kingdom*
[2]*Department of Physics, Swansea University, Singleton Park, Swansea SA2 8PP, United Kingdom*
[3]*Department of Mechanical Engineering, University of Cyprus, Nicosia 1678, Cyprus*
(Received 4 November 2009; revised manuscript received 4 February 2010; published 4 March 2010)

A 2+1-dimensional fermion field theory is proposed as a model for the low-energy electronic excitations in monolayer graphene. The model consists of $N_f=2$ four-component Dirac fermions moving in the plane and interacting via a contact interaction between charge densities. For strong couplings there is a continuous transition to a Mott insulating phase. We present results of an extensive numerical study of the model's critical region, including the order parameter, its associated susceptibility, and the quasiparticle propagator. The data enable an extraction of the critical exponents at the transition (including the dynamical critical exponent) which are hypothesized to be universal features of a quantum critical point. The relation of our model with others in the literature is discussed along with the implications for physical graphene following from our value of the critical coupling.

DOI: 10.1103/PhysRevB.81.125105 PACS number(s): 71.10.Fd, 11.10.Kk, 11.15.Ha, 73.90.+f

I. INTRODUCTION

There has been much recent interest in the remarkable electronic properties of graphene[1] (see also a recent, comprehensive review in Ref. 2). It appears that they arise from the low-energy spectrum of excitations being equivalent to that of a two-dimensional gas of relativistic fermions, with the case of undoped (i.e., neutral) graphene corresponding to zero net particle number. In brief, for a carbon monolayer with one mobile electron per atom, a simple tight-binding model predicts a linear dispersion relation centered on zeroes located at the six corners of the first Brillouin zone. It is possible to rewrite the Hamiltonian for single-particle excitations in Dirac form with $N_f=2$ flavors of four-component spinor ψ, the counting of degrees of freedom coming from 2 C atoms per unit cell $\times 2$ zeroes per zone $\times 2$ physical spin components per electron. Electron propagation within the monolayer is thus relativistic, albeit with speed $v_F \approx c/300$.

The charge carriers in graphene can be either electrons ("particles") or holes ("antiparticles") and are characterized by a very high value of mobility $\mu=\sigma/ne$ (where σ is electrical conductivity and n the carrier density), more than twice that of the highest mobility conventional semiconductor, and several orders of magnitude greater than a typical metal at room temperature. This gives graphene the potential to be of great technological significance in the construction of fast electronic devices. The naive tight-binding model suggests, and experiments with graphene based on a SiO_2 substrate confirm, that graphene remains a conductor (technically a semimetal) for all values of the gate voltage, i.e., even when the carrier density formally vanishes because there is no gap in the energy spectrum $E(k)$ at the Dirac points. The presence of a small gap would, however, be extremely valuable for electronics applications because it would increase the effective on-off current flow ratio needed for device stability.[3]

More sophisticated theoretical approaches to graphene must take interelectron interactions into account. In this paper we build upon an approach which treats the low-energy fermion excitations using a 2+1-dimensional relativistic quantum field theory.[4–6] The interaction between electrons is assumed to be due to a Coulomb potential, which in undoped (i.e., neutral) graphene is unscreened due to the vanishing density of states at $E=0$. Because $v_F \ll c$ this Coulomb interaction can be treated as "instantaneous," meaning that the field theory is necessarily nonlocal. The strength of the Coulomb interaction is variable since it depends on the dielectric constant ε of the underlying substrate. It can be parametrized by an effective fine-structure constant

$$\alpha = \frac{e^2}{4\pi\varepsilon\varepsilon_0\hbar v_F} \sim O(1) \tag{1}$$

so that the problem is strongly interacting. The possibility then opens up of the disruption of the free-field ground state by an excitonic condensate, i.e., one formed from tightly bound electron-hole pairs with the effect of opening up a gap $\Delta>0$ at the Dirac point and making the ground state of undoped graphene a Mott insulator.

The analogous phenomenon in particle physics is described using different language: we say that the global chiral symmetry of the model, which prevents generation of a fermion mass through quantum corrections to all orders in perturbation theory, is spontaneously broken by the formation of a chiral condensate. Dynamical mass generation is therefore inherently nonperturbative and must be addressed either by self-consistent analytic methods or, as in this paper, by numerical simulation of a lattice-regularized version of the field theory. To date there have been two distinct approaches taken. In a series of papers, Drut and Lähde[7–9] have simulated a formulation of the graphene field theory based on lattice gauge theory in which electrostatic degrees of freedom are formulated on a 3+1-dimensional lattice while the electron fields are restricted to a 2+1-dimensional slice. By contrast, our formulation[10] is entirely 2+1 dimensional and is in essence a noncovariant form of the Thirring model. Both numerical calculations support the hypothesis proposed in Ref. 6 that the semimetal and insulator phases are separated by a line of second-order phase transitions in the

(α, N_f) plane, starting at a point (∞, N_{fc}) and running in the direction of decreasing α and decreasing N_f. A very similar situation pertains in the $2+1d$ Thirring model.[11,12] In Ref. 10 we studied chiral symmetry breaking with variable N_f in the strong-coupling limit and estimated $N_{fc}=4.8(2)$. Each point on the line with integer $N_f<N_{fc}$ defines a quantum critical point (QCP) whose properties are characterized by a set of N_f-dependent critical exponents [in Ref. 6 the identification of the QCP was restricted to the case (∞, N_{fc})].

In the current paper we present an extensive numerical study of the semimetal-insulator phase transition for the case $N_f=2$ which is of direct physical interest; only preliminary results were available in Ref. 10. The graphene model we study will be presented in detail, both as a continuum field theory and as a lattice model, in the following section but it is appropriate to preface that with some remarks. Because our approach is based on a local quantum field theory in $2+1d$, it is unable to capture the long-range $1/r$ nature of the unscreened Coulomb potential assumed in Refs. 4–6. We have argued in Ref. 10 that this is unimportant in the strong-coupling limit $\alpha \to \infty$ where electron-hole pair polarization effects dominate the long-range physics; however for finite α our model is in principle different both from the continuum approaches[4–6] and the lattice gauge theory approach of Refs. 7–9. We do not exclude the possibility, however, that the universal behavior at the QCP remains the same, even for $N_f<N_{fc}$.

There are two main benefits of our approach. First, the simplicity of our model and the fact that it is formulated directly on a $2+1d$ space-time lattice mean that we have been able to perform accurate simulations on a range of system sizes $L_s^2 \times L_t$, yielding control over finite-size artifacts and hence access to the model's critical properties. Second, the fact that our model is *not* a gauge theory permits a definition of the quasiparticle correlation function without any need for gauge fixing, which is known to be a major source of statistical noise in similar model systems, e.g., Ref. 13. We are able here to present the numerical study of the quasiparticle propagator, which both explicitly demonstrates gap generation as the coupling strength g^2 is increased beyond g_c^2 and broadens the scope of the critical analysis; we are able to present an estimate for the dynamical critical exponent z which governs the different scaling of the correlation length in spacelike and timelike directions.

The remainder of the paper is organized as follows. In Sec. II we lay out the model to be studied in both continuum and lattice formulations, and discuss its relation with other models studied in the literature and its applicability to graphene. Our numerical results are presented in Sec. III: Sec. III A focuses on the chiral order parameter and its associated susceptibility, and fits data to a renormalization-group inspired critical equation of state yielding estimates for the critical coupling and exponents δ and β; Sec. III B presents an analysis of the quasiparticle propagator and shows how both the gap Δ and the renormalized Fermi velocity v_{FR} may be extracted; finally Sec. III C presents a fit to a similarly motivated equation of state for $\Delta(m, g^2)$ which along with the assumption of hyperscaling permits an estimate of the dynamical critical exponent z. We summarize our findings for the critical parameters in Sec. IV and also attempt to relate our value for g_c^2 to estimates of α_c in the literature.

II. FORMULATION AND INTERPRETATION OF THE MODEL

Our starting point is a model of relativistic Dirac fermions moving in $2+1$ dimensions and interacting via an instantaneous Coulomb interaction. In Euclidean metric the action is[4–6]

$$S_1 = \sum_{a=1}^{N_f} \int dx_0 d^2x (\bar{\psi}_a \gamma_0 \partial_0 \psi_a + v_F \bar{\psi}_a \vec{\gamma} \cdot \vec{\nabla} \psi_a + iV \bar{\psi}_a \gamma_0 \psi_a) + \frac{1}{2e^2} \int dx_0 d^3x (\partial_i V)^2, \tag{2}$$

where e is the electron charge, v_F the Fermi velocity, V the electrostatic potential, and the 4×4 Dirac matrices satisfy $\{\gamma_\mu, \gamma_\nu\}=2\delta_{\mu\nu}$, $\mu=0,1,2$. For monolayer graphene the correct number of fermion flavors $N_f=2$. The momentum-space propagator for the V-field D_1, which couples conserved charge densities $\bar{\psi}\gamma_0\psi$ at differing spacetime points, is given by

$$D_1(p) = \left[\frac{2|\vec{p}|}{e^2} + \frac{N_f}{8} \frac{|\vec{p}|^2}{(p^2)^{1/2}} \right]^{-1}, \tag{3}$$

where the first term in brackets on the right-hand side is the classical Coulomb interaction and the second is the leading quantum correction in the large-N_f limit, describing screening due to particle-hole virtual pairs. Note that $p^2=p_0^2+v_F^2|\vec{p}|^2$. The relative importance of quantum versus classical effects may be parametrized by the ratio λ of the two terms in the static limit $p_0 \to 0$; in SI units

$$\lambda = \frac{e^2 N_f}{16 \varepsilon \varepsilon_0 \hbar v_F} \simeq \frac{1.4 N_f}{\varepsilon}, \tag{4}$$

where $\varepsilon > 1$ is the dielectric constant of the underlying substrate.

For sufficiently large interaction strength the description in terms of massless relativistic excitations may be disrupted by condensation of bound fermion-hole pairs in the ground state, signaled by an order parameter $\langle \bar{\psi}\psi \rangle \neq 0$, with the result that a gap appears in the fermion spectrum. Physically this corresponds to a transition from a conductor to an insulator; in the language of particle physics the same phenomenon, resulting in a dynamical generation of a particle mass, is known as chiral symmetry breaking. As this transition occurs at zero temperature, the model predicts a finite sequence of QCPs whose properties at the critical interaction strength $\lambda_c(N_f)$ are sensitive to the value of N_f:[6] the sequence will terminate for N_{fc} (not necessarily integer) defined by $\lambda(N_{fc})=\infty$.

This situation has motivated us to explore a related but distinct model for graphene, with action[10] (in units where $v_F=1$)

$$S_2 = \sum_{a=1}^{N_f} \int dx_0 d^2x \left[\bar{\psi}_a \gamma_\mu \partial_\mu \psi_a + iV\bar{\psi}_a \gamma_0 \psi_a + \frac{1}{2g^2} V^2 \right] \quad (5)$$

This model resembles the $2+1d$ Thirring model,[11,12] a four-fermi model known to exhibit a sequence of N_f-dependent QCPs as the coupling strength g^2 is varied. The relation with Eq. (2) is clarified by inspection of the V propagator,

$$D_2(p) = \left[\frac{1}{g^2} + \frac{N_f}{8} \frac{|\vec{p}|^2}{(p^2)^{1/2}} \right]^{-1}. \quad (6)$$

Since the quantum correction is identical, models (2) and (5) should yield the same physics in the large-λ limit, which can be reached as either $N_f \to \infty$ or $g^2, e^2 \to \infty$. Indeed, in Ref. 10 we used this property to predict the critical number of flavors $N_{fc}=4.8(2)$ above which model (2) remains a semimetal for all g^2. Thus graphene with $N_f=2$ is predicted to be a Mott insulator for sufficiently strong interelectron coupling. For finite N_f models (2) and (5) are distinct, although we may still hope they describe similar physics for λ not too small.

Let us discuss this point a little further. The principal difference between Eqs. (3) and (6) occurs at large distances, i.e., $\lim_{r\to\infty} D_1(r) \propto r^{-2}$, indicating that the long-range Coulomb interaction is not screened, whereas D_2 is finite ranged, being cutoff for $r \gtrsim O(g^2)$. It is important to understand whether the modification $D_1 \mapsto D_2$ changes the physics in any essential way, e.g., by defining a model in a different universality class. We will be unable to answer this question definitively with the simulation results presented here but note that in the model approach of Ref. 5 which predicts dynamical symmetry breaking, the relevant momentum range responsible for gap generation is $|\vec{p}| \gg \Delta / v_F$, implying that it is the short-ranged behavior of D which governs the properties of the QCP. In addition, we note that unlike the instantaneous approximation used in that work D_2 correctly incorporates the p_0 behavior of the vacuum polarization function.

In this paper we will use numerical simulations of a lattice model based on a discretised version of Eq. (5) to study the semimetal-insulator transition for the physical value $N_f=2$. The lattice model is formulated in terms of single-component Grassmann fields $\chi, \bar{\chi}$ defined on the sites x of a three-dimensional cubic lattice by the action

$$S_{\text{latt}} = \sum_{x\mu} \bar{\chi}_x \frac{\eta_{\mu x}}{2} [(1 + \delta_{\mu 0}\sqrt{2g^2} e^{iV_x}) \chi_{x+\hat{\mu}} - (1 + \delta_{\mu 0}\sqrt{2g^2} e^{-iV_{x-\hat{0}}}) \chi_{x-\hat{\mu}}] + m \sum_x \bar{\chi}_x \chi_x. \quad (7)$$

The sign factors $\eta_{x\mu} \equiv (-1)^{x_0 + \cdots + x_{\mu-1}}$ ensure that in the long-wavelength limit the first (anti-Hermitian) term in S_{latt} describes the Euclidean propagation of $N_f=2$ flavors of relativistic fermion described by four-component spinors.[14] The bare fermion mass m provides a IR regulator for modes which would otherwise be massless in the limit of weak interactions. The hopping terms in S_{latt} involve the auxiliary boson field V_x which is formally defined on the *timelike* links connecting sites x with $x+\hat{0}$. For further details of the relation between the actions [Eqs. (5) and (7)] we refer the reader to Refs. 10 and 11 [in particular, for $N_f=2$ the action, Eq. (7), can be recast in a "noncompact" form yielding identical physics, whose relation to Eq. (5) is more manifest]. Because we restrict our consideration to an integer number of fermion flavors in this paper we were able to perform the simulation using a well-established numerical method called the hybrid Monte Carlo (HMC) algorithm, which generates equilibrated ensembles of field configurations $\{V\}$ with no systematic bias.[11,15]

Since our initial paper,[10] results from simulation of an alternative lattice approach to the graphene model (2) have appeared.[7–9] This formulation is based on lattice gauge theory in which the degrees of freedom corresponding to the electrostatic potential V are formulated on a $3+1d$ lattice while the electron degrees of freedom are confined to a $2+1d$ "braneworld." This in principle gives a more faithful rendering of the physics encapsulated in Eqs. (2) and (3). The principal result is a prediction for the critical coupling corresponding to the semimetal-insulator transition; for $N_f=2$ the value

$$\lambda_c^{DL} = 1.70(2) \quad (8)$$

was obtained. This result is intriguing because it lies between the values $\lambda \simeq 1.25$ expected for graphene on an SiO_2 substrate, which experiments have shown to be a conductor, and $\lambda \simeq 3.4$ [cf. Eq. (4)] for freely suspended graphene, which is accordingly predicted to be an insulator. The necessity to store and evolve variables on an extra dimension is clearly a computational burden the action [Eq. (7)] evades; however for current purposes the main advantage we claim for our approach is that it permits a straightforward means to measure the quasiparticle propagator, as presented below in Sec. III B, without the need for gauge fixing.

Before finishing we wish to compare our model with another approach to electron transport on a honeycomb lattice, namely, the Hubbard model. This model leads to the same kinetic term in the long-wavelength limit as that of Eq. (2) but now with a repulsive on-site interaction between electrons of opposite spin, the last restriction being due to the exclusion principle. On a square lattice the Hubbard model is predicted to have an antiferromagnetic insulating ground state for any interaction strength U, however small. On the honeycomb, the distinct nature of the low-energy excitation spectrum results in a transition between antiferromagnetic and paramagnetic phases at a nonzero U_c, which appears to coincide with a semimetal-insulator transition akin to that discussed here.[16] In our model, however, the Coulomb interaction between charge carriers is spin independent and acts over arbitrary separations so is not constrained by the exclusion principle; the correlations between spins discussed in Ref. 16 are therefore absent. Note that a model including both Hubbard and Coulomb interactions was studied in Ref. 17.

Let us finish this section by discussing the behavior we expect of model (7) and how it might relate to physical graphene. In the limit $m \to 0$ the model has a global chiral symmetry $\chi_x \mapsto \exp i\alpha\varepsilon_x \chi_x; \bar{\chi}_x \mapsto \exp i\alpha\varepsilon_x \bar{\chi}_x$, where the sign factor $\varepsilon_x \equiv (-1)^{x_0+x_1+x_2}$ distinguishes odd and even sublattices: the model studied in Refs. 7–9 has the identical symmetry. For N_f flavors the pattern of symmetry breaking ex-

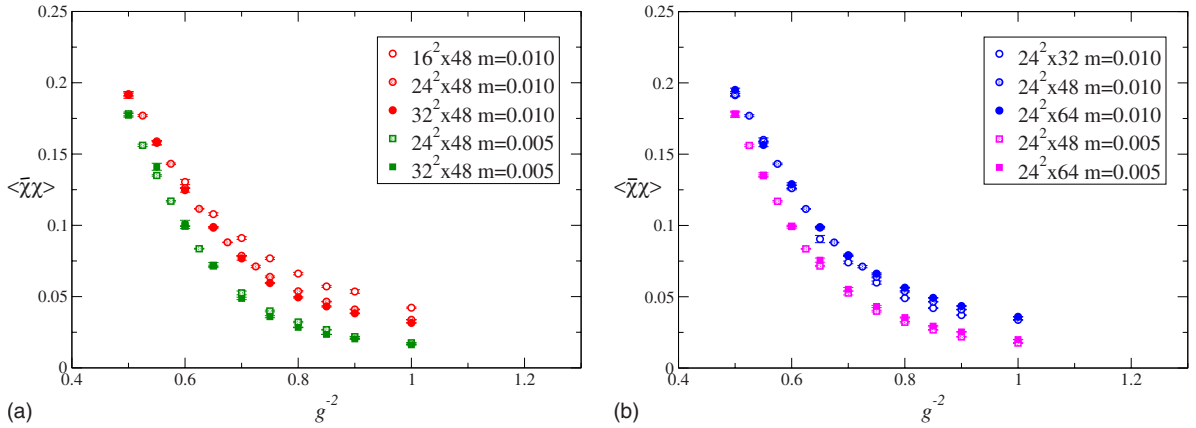

FIG. 1. (Color online) $\langle\bar{\chi}\chi\rangle$ vs g^{-2} for $m=0.01$ calculated on (a) $L_s^2\times 48$ lattices and (b) $24^2\times L_t$ lattices, showing finite-size effects.

pected for the continuum models (2) and (5) is $U(2N_f)\rightarrow U(N_f)\otimes U(N_f)$, whereas away from the continuum limit the pattern for Eq. (7) is $U(\frac{N_f}{2})\otimes U(\frac{N_f}{2})\rightarrow U(\frac{N_f}{2})$. By analogy with the Thirring model,[11] we expect that for large values of the coupling g^2 the symmetry will be dynamically broken as signaled by a nonvanishing condensate $\langle\bar{\chi}\chi\rangle \equiv V^{-1}\partial \ln \mathcal{Z}/\partial m\neq 0$ but that the symmetry will be restored in a continuous phase transition at some critical coupling g_c^{-2}. This transition between the two phases defines a UV-stable fixed point of the renormalization group and the fixed-point theory is thus uniquely specified by a set of critical exponents—one of the main goals of the paper, presented in Sec. III A, is to determine both the critical g_c^{-2} and the set of exponents by numerical means. The fixed-point theory should describe the low-energy excitations of physical graphene in the continuum limit, reached either from the insulating phase as $g^{-2}\nearrow g_c^{-2}$, $\langle\bar{\chi}\chi\rangle\rightarrow 0$ or from the conducting phase as $g^{-2}\searrow g_c^{-2}$, $m\rightarrow 0$. As we shall see below, it may be possible to relate the value of g_c^{-2} to λ as defined via Eq. (4). The applicability of the model to graphene, however, rests on the hypothesis that the low-energy excitations and their interactions in graphene share its symmetries, and that the physical parameters are such that graphene lies within the basin of attraction of the fixed point. Ultimately this must be settled by experiment.

III. NUMERICAL RESULTS

Preliminary simulations with $N_f=2$ presented in Ref. 10 showed evidence for a crossover from strong- to weak-coupling behavior at $g^{-2}\approx 0.6$. Accordingly, we have undertaken a refined campaign of simulation on system sizes $L_s^2\times L_t$ with L_s ranging from 16 to 48 and L_t ranging from 48 to 84; the bare mass m was varied between 0.0025 and 0.025. Because the action [Eq. (7)] does not treat space and (Euclidean) time directions equivalently, it is useful to explore the consequences of independently varying L_s and L_t: however, the most detailed coverage of the g^{-2} axis was obtained on $24^2\times 48$.

A. Equation of state

In the vicinity of a second-order phase transition the order parameter over a range of couplings g^{-2} and small source values m can be described by an equation of state of the form

$$m=\langle\bar{\chi}\chi\rangle^{\delta}\mathcal{F}(t\langle\bar{\chi}\chi\rangle^{-1/\beta})=At\langle\bar{\chi}\chi\rangle^{p}+B\langle\bar{\chi}\chi\rangle^{\delta}+O(t^2\langle\bar{\chi}\chi\rangle^{p-1/\beta}), \tag{9}$$

where g_c^{-2} is the critical coupling, $t\equiv g^{-2}-g_c^{-2}$, $\mathcal{F}$ is a universal scaling function, δ the critical exponent describing the order parameter's response at criticality to a small applied source m, β the exponent governing the scaling of the order parameter for $m=0$ as $t\rightarrow 0_-$, and $p\equiv\delta-1/\beta$. Order-parameter data taken in the thermodynamic limit can be fitted to Eq. (9) to extract g_c^{-2}, δ, and p. In practice we need to make assumptions about the width of the "scaling window" in g^{-2} and m where the subleading corrections in Eq. (9) can be safely ignored and we also need to carefully monitor the effects of working with finite L_s and L_t.

First let's discuss finite-volume effects. Since model (7) has an anisotropic action, we cannot *a priori* exclude the possibility of correlation lengths in spatial and temporal directions diverging with distinct exponents ν_s and ν_t.[18] In previous work we have attempted to incorporate this possibility via a correction to the equation of state fit but the complicated nature of the finite-volume scaling model made these fits of questionable value given the range of simulation volumes available to us. Here we take a more pragmatic approach and compare order-parameter data for two different bare masses at fixed L_t and varying L_s in Fig. 1(a) and vice versa in Fig. 1(b). The plots reveal the very different nature of the finite-size effects in each case: $\langle\bar{\chi}\chi\rangle$ rises as L_t is increased, corresponding to the zero-temperature limit, but falls as the thermodynamic limit $L_s\rightarrow\infty$ is approached. Moreover, in both cases the effects are greater in the symmetric phase, i.e., at larger values of g^{-2}. We will proceed by using the observation that in the restricted range $0.525\leq g^{-2}\leq 0.65$ the data for $m=0.005$ ($0.525\leq g^{-2}\leq 0.70$ for $m\geq 0.01$) on $24^2\times 48$ are free from finite-size effects almost within statistical error.

Table I shows sample fits to Eq. (9) to $O(t)$ for order-parameter data taken on a $24^2\times 48$ lattice and shows how the fit quality improves as data far from criticality are successively excluded. We also tried excluding low-mass points as these are most susceptible to finite-volume effects. It is com-

TABLE I. Various fits to the equation of state [Eq. (9)] for data taken on $24^2 \times 48$.

Fit	No.	g_c^{-2}	δ	p	χ^2/dof
$0.525 \le g^{-2} \le 0.90$ (all m)	69	0.608(2)	2.66(2)	1.252(4)	6.9
$0.55 \le g^{-2} \le 0.80$ (all m)	55	0.607(2)	2.68(3)	1.261(9)	4.0
$0.525 \le g^{-2} \le 0.65$ (m=0.005)	43	0.609(2)	2.66(3)	1.245(11)	2.7
$0.525 \le g^{-2} \le 0.675$ (m=0.0075)					
$0.525 \le g^{-2} \le 0.70$ ($m \ge 0.01$)					
$0.525 \le g^{-2} \le 0.70$ ($m \ge 0.0075$)	37	0.600(3)	2.80(5)	1.285(14)	2.3

forting that the fitted values of the critical parameters are quite stable as the scaling window is so varied. Our preferred fit is the third row of Table I, which includes as much data as possible consistent with preserving acceptable fit quality:

$$g_c^{-2} = 0.609(2); \quad \delta = 2.66(3); \quad p = 1.245(11) \Rightarrow$$

$$\beta = 0.71(2). \tag{10}$$

The fitted equation of state is plotted in Fig. 2.

We also experimented with fits with an extra free parameter modeling an $O(t^2)$ correction to Eq. (9); these fits indicated a slightly larger value of g_c^{-2} but despite the extra free parameter did not yield appreciably better χ^2 values. Moreover, the resulting equation of state clearly failed to be physically reasonable in the symmetric phase: since $\delta - \frac{2}{\beta} < 0$ from Eq. (10), the $O(t^2)$ term rapidly becomes numerically dominant here. In support of this, Fig. 3 plots order-parameter data taken on $24^2 \times 48$ using axes chosen, using the critical parameters [Eq. (10)], to effect data collapse onto the scaling function $\mathcal{F}$ which is seen to be linear to very good approximation.

Finally we examine another probe of the critical point, the ratio of transverse to longitudinal susceptibilities $\chi_\ell / \chi_t \equiv \partial \ln \langle \bar{\chi}\chi \rangle / \partial \ln m$.[8,11] There are two spin-0 particle-hole channels with opposite intrinsic parities, which by analogy with mesons in particle physics we refer to as σ (parity +) and π (parity −). In the $m \to 0$ limit, in the conducting phase the two states are related by a U(1) global chiral symmetry and are degenerate; in the insulating phase, by contrast, the symmetry is spontaneously broken and the π channel therefore contains a massless pole by Goldstone's theorem. Since χ_ℓ / χ_t is simply the ratio of the integrated σ propagator to the integrated π propagator, we expect it to tend to unity as $m \to 0$ in the conducting phase and to zero in the insulating phase. Exactly at criticality, however, the ratio is m independent and takes the value $1/\delta$.[19] Figure 4 plots χ_ℓ / χ_t vs m evaluated on a $24^2 \times 48$ lattice, including contributions from diagrams with both connected and disconnected fermion lines as detailed in Ref. 11. The data taken at $g^{-2} = 0.60, 0.625$ are approximately m independent, especially for larger m, and bracket the value of δ^{-1} obtained from the equation of state fit, strengthening our confidence in the values of the critical parameters in Eq. (10).

B. Quasiparticle dispersion

One of the main motivations for the choice of model (7) is that since it has no manifest gauge symmetry, there is no requirement to fix a gauge in order to define or measure a correlation function such as the fermion propagator. This has enabled us to perform the first numerical simulation of the quasiparticle excitation spectrum in graphene.

The fermion excitation spectrum of the model is accessed via analysis of the Euclidean timeslice propagator $C_f(\vec{p},t)$ defined by

$$C_f(\vec{p},t) = \sum_{\vec{x} \text{ even}} \langle \chi(\vec{0},0) \bar{\chi}(\vec{x},t) \rangle e^{-i\vec{p}\cdot\vec{x}}, \tag{11}$$

where "even" refers to sites with spatial coordinate $\vec{x}$ obeying $(-1)^{x_1} = (-1)^{x_2} = 1$ and the components of $\vec{p}$ take values

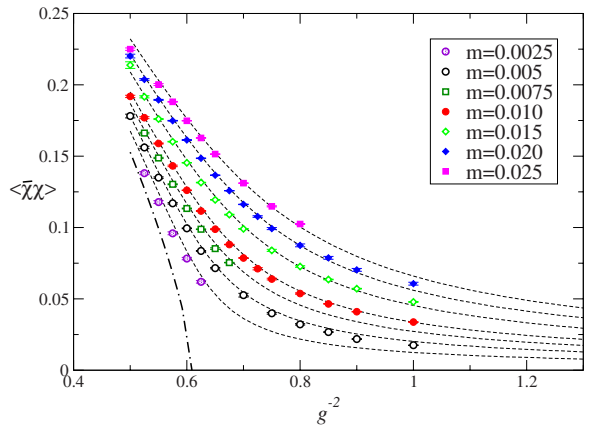

FIG. 2. (Color online) Fit to Eq. (9) to order-parameter data taken on $24^2 \times 48$. The function in the $m \to 0$ limit is also shown.

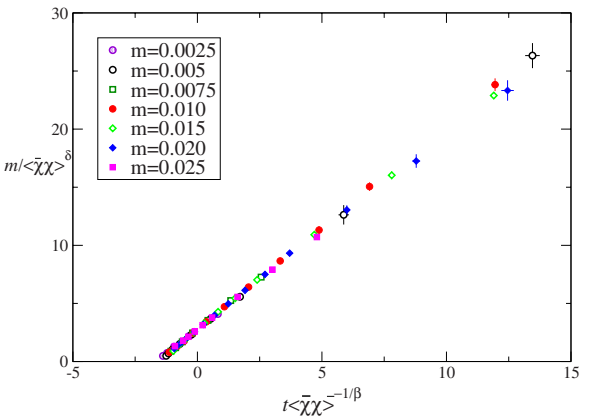

FIG. 3. (Color online) Plot of $m/\langle \bar{\chi}\chi \rangle^{\delta}$ vs $(g^{-2} - g_c^{-2}) \langle \bar{\chi}\chi \rangle^{-1/\beta}$ using the critical parameters [Eq. (10)].

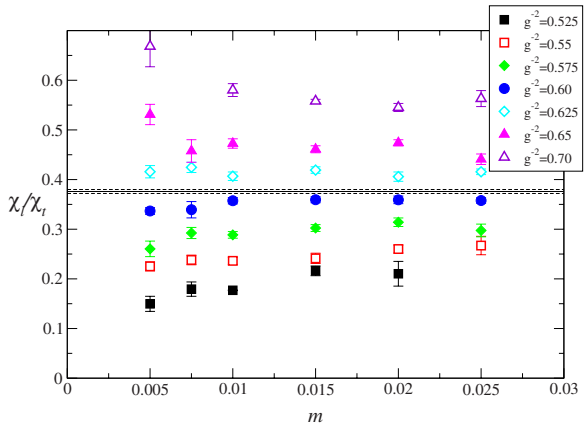

FIG. 4. (Color online) Susceptibility ratio χ_ℓ/χ_t vs m for various g^{-2} in the critical region. The fitted value of δ^{-1} from Eq. (10) is shown as a horizontal band.

$2\pi n/L_s$, with $n=0,1,\ldots,L_s/4$. This restriction improves the signal-to-noise ratio and originates in the observation that the action [Eq. (7)] is invariant only under translations by an even number of lattice spacings. The energy $E(\vec{p})$ is then extracted by a fit of the form

$$C_f(\vec{p},t) = B(e^{-Et} + e^{-E(L_t-t)}), \tag{12}$$

where in this case only data with t odd were used since this yielded the best fits across the whole range of g^{-2} (it can be shown that $\lim_{m\to 0} C_f=0$ for even t in the conducting phase).

We measured $E(\vec{p})$ for $\vec{p}=(p_1,0)$ on $32^2\times 48$ for $g^{-2}=0.55,0.6,0.7,0.8$ and additionally on 48^3 for $g^{-2}=0.8,0.9$, using m ranging from 0.005 to 0.03. The resulting dispersions for the latter two systems at $m=0.005$ are shown in Fig. 5. For small p and m the dispersion starts out linear to good approximation and then flattens out to have zero slope at the effective Brillouin-zone edge at $p=\frac{\pi}{2}$; this flattening is a discretization artifact with no physical significance. To proceed we parametrize the dispersion relation using

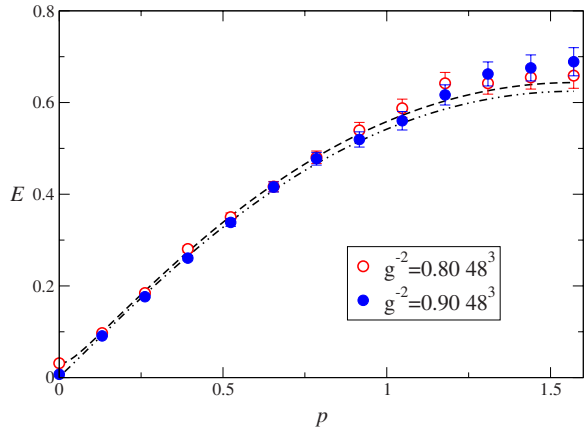

FIG. 5. (Color online) Dispersion relation $E(p)$ as measured on a 48^3 lattice with $m=0.005$.

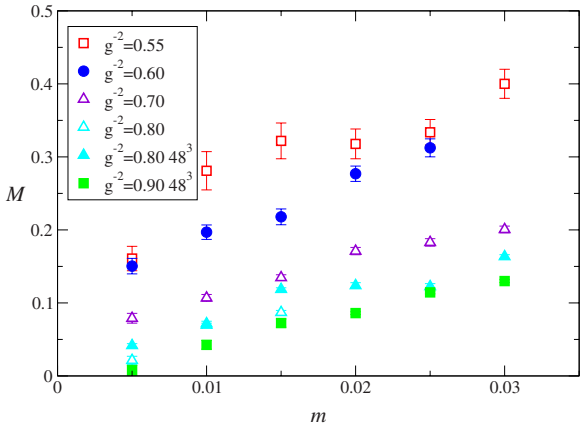

FIG. 6. (Color online) The fitted parameter M vs m for various g^{-2}.

$$E(p) = A\ \sinh^{-1}(\sqrt{\sin^2 p + M^2}), \tag{13}$$

where for $A=1$ and $M=m$ the exact result for noninteracting lattice fermions is recovered. Two sample fits are shown in Fig. 5. For small M we can interpret $E(0)\equiv\Delta\approx AM$ as the quasiparticle mass (or gap), and for small p in the limit $M\to 0$ then $dE/dp\approx A$ is the physical Fermi velocity v_{FR}. Results for A and M as functions of m are shown in Figs. 6 and 7.

The results for M are broadly consistent with our identification of the critical coupling. For $g^{-2}<g_c^{-2}\simeq 0.6$, Fig. 6 supports $\lim_{m\to 0} M\neq 0$, signaling the generation of a gap via spontaneous chiral symmetry breaking. For weaker couplings the data can be plausibly extrapolated in the same limit to $M=0$, signaling a chirally symmetric, conducting phase. Note that throughout the critical region $\Delta \gg m$, indicating large mass renormalization due to strong interactions even in the symmetric phase. In Sec. III C below we will present further results for M for a range of m in the critical region.

Figure 7 shows that despite some noise in the data the parameter A and hence the physical Fermi velocity v_{FR}, is both m and g^{-2} independent in the critical region, taking a numerical value ≈ 0.7. We interpret this as being due to a

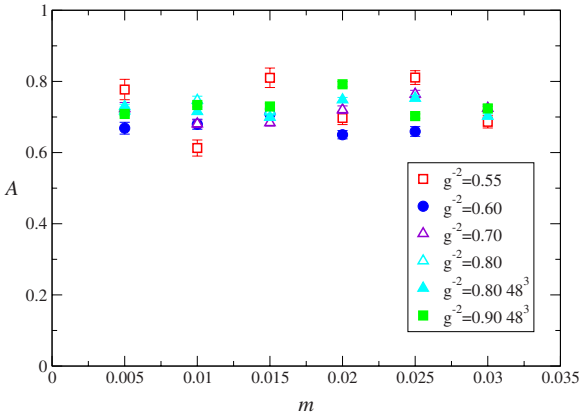

FIG. 7. (Color online) The fitted parameter A vs m for various g^{-2}.

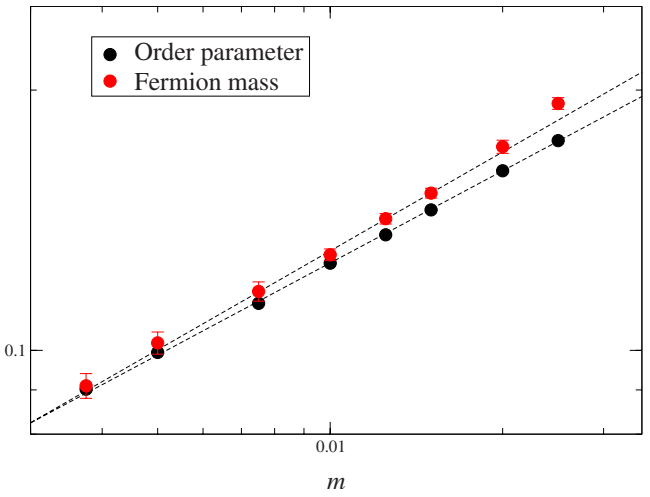

FIG. 8. (Color online) $\langle\bar{\chi}\chi(m)\rangle$ and $M(m)$ at $g^{-2}=0.6$ on $24^2\times 48$.

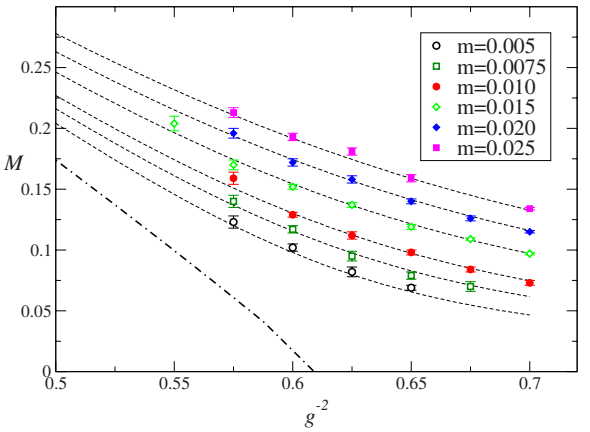

FIG. 9. (Color online) Fit to Eq. (16) for $M(m)$ data taken on $24^2\times 48$.

renormalization of the bare Fermi velocity $v_F\equiv 1$ due to quantum effects. This in principle needs be taken into account when we attempt to assign a physical value to the critical coupling g_c^{-2} in Sec. IV. This result is interesting because analytic calculations based on weak coupling and/or large N_f predict that $v_{FR}>v_F$,[20] whereas a self-consistent treatment based on a short-ranged interelectron interaction finds v_{FR} decreasing montonically to zero as the QCP is approached from weak coupling.[21]

C. Dynamical critical exponent

In this section we take a closer look at correlations in the critical system, both via a high statistics study (typically several thousand HMC trajectories) at $g^{-2}=0.6$, close to the critical value reported in Eq. (10), and a refined study of the quasiparticle mass parameter M in the critical region. All results are from simulations on $24^2\times 48$ lattices. Because model (7) treats space and time differently, correlation lengths defined in spatial and temporal directions can exhibit different critical scaling, leading to two distinct exponents defined via[18]

$$\xi_s \propto |t|^{-\nu_s}; \quad \xi_t \propto |t|^{-\nu_t}. \tag{14}$$

Our goal in this section is to constrain the value of the dynamical critical exponent $z\equiv \nu_t/\nu_s$ relating spacelike to timelike correlations.

Figure 8 shows data for both the order parameter $\langle\bar{\chi}\chi\rangle$ and mass parameter M defined by Eq. (13) as a function of m on a log-log plot. The linear nature of the plots supports a power-law scaling,

$$\langle\bar{\chi}\chi\rangle \propto m^{1/\delta}; \quad M \propto m^{\nu_t/\delta\beta}, \tag{15}$$

where δ and β coincide with the definitions implicit in Eq. (9) and the exponent ν_t is the one relevant for the extraction of spectral properties via Eq. (12) from correlations in the Euclidean time direction. Least-squares fits (excluding $m=0.025$) yield $\delta=2.85(1)$; $\frac{\nu_t}{\delta\beta}=0.38(2)$. The mismatch between this value for δ and that of Eq. (10) extracted from the equation of state is ascribed to the actual value of g_c^{-2} lying slightly above 0.6, as suggested by Fig. 4.

Figure 9 shows results for the quasiparticle mass parameter M for a range of m and g^{-2} values in the critical region. We have fitted these data with a relation inspired by the equation of state [Eq. (9)],

$$m = AtM^{\beta p/\nu_t} + BM^{\delta\beta/\nu_t}, \tag{16}$$

which with $M\propto\xi_t^{-1}$ understood recovers Eq. (14) in the limit $m\to 0$ and is consistent with Eq. (15) when $t=0$. A fit to 33 datapoints with g_c^{-2} fixed by Eq. (10) yields

$$\frac{\delta\beta}{\nu_t} = 2.25(5); \quad \frac{\beta p}{\nu_t} = 1.16(6) \tag{17}$$

with χ^2 per degree of freedom of 1.0.

It is now time to discuss the possible anisotropy at $g^{-2}=g_c^{-2}$ in more detail. As mentioned above, the ratio $z=\nu_t/\nu_s$ defines the *dynamical critical exponent*, which is an important characteristic of a QCP. In particular, the critical dispersion relation is modified to be of the form $E\propto p^z$, which has important implications for the stability of quasiparticles; energy and momentum conservation make it impossible, in an inelastic collision, for a quasiparticle to decay into constituents with smaller E and p if $z<1$.[6]

The results in this section permit an estimate of z via the following indirect argument. First, we use the exponent values from Eq. (17) and δ,β from Eq. (10) to estimate

$$\nu_t = 0.80(3). \tag{18}$$

Next, we use a modified hyperscaling relation[18,22]

$$\nu_t + (d-1)\nu_s = \beta(\delta+1), \tag{19}$$

where $d=3$ is the number of space-time dimensions to estimate

$$\nu_s = 0.89(3), \tag{20}$$

leading to

$$z = 0.90(5). \tag{21}$$

This result is tantalizing since although it hints at $z<1$ it eliminates neither the value $z\approx 0.8$ based on a leading-order large-N_f calculation in the strong-coupling limit[6] nor the general result $z\equiv 1$ claimed for systems at a QCP with $d<4$ interacting via a Coulomb potential.[23]

IV. DISCUSSION

The main result of this paper is that by numerical means we have identified a quantum critical point, corresponding to a semimetal-insulator transition, for a model with $N_f=2$ flavors of Dirac fermion sharing many symmetries with a low-energy effective theory of monolayer graphene. We have been able to identify critical exponents characterizing the transition, as summarized in Eq. (10); the most robust prediction, emerging from a fit to the equation of state and supported by both a calculation of the susceptibility ratio χ_ℓ/χ_t and a direct study of the scaling of the order parameter against m at $g^{-2}\approx g_c^{-2}$, is that the exponent $\delta=2.66(3)$. This is significantly different from the value $\delta=5.5(3)$ obtained in the strong-coupling limit at $N_f=N_{fc}=4.8(2)$,[10] demonstrating that the universality class the model falls into is N_f dependent. A similar picture has emerged from numerical simulations of the $2+1d$ Thirring model,[11,12] where it has been shown that δ *increases* with N_f. Drut and Lähde[9] have reported the same trend from numerical simulations of their model with $N_f=0,2,4$. However, their most recent value for $\delta(N_f=2)=2.26(6)$ is significantly different from ours, so it remains unclear whether the two models lie in the same universality class or whether the long-range interaction present in the model of[9] but not here has a decisive effect.

We have also presented results for quasiparticle propagation, finding evidence for a gap developing spontaneously in the spectrum for $g^{-2}<g_c^{-2}$ as $m\to 0$. In addition, analysis of correlations at nonzero momentum has enabled us to roughly calculate the renormalization of the Fermi velocity v_F. We reiterate that in our model the fermion propagator is uniquely defined and readily calculable; in the original model (2) the presence of a local gauge symmetry makes analysis of quasiparticle propagation potentially problematic both theoretically and numerically.

We have also outlined a method to obtain the dynamical critical exponent z, an important characteristic of any QCP, using scaling and hyperscaling arguments. Unfortunately the inevitable accumulation of errors in such an indirect approach precludes us at this stage from conclusively deciding whether $z<1$ or not. This issue is of theoretical interest since there are general arguments to claim z is exactly one for Coulombic systems[23] (of course, strictly our model is not in this class). In this respect a more direct attempt to extract z via measurements of the quasiparticle dispersion $E(p)$ on lattices with a large spatial dimension giving enhanced momentum resolution may prove interesting.

Another interesting direction for future simulations is the impact of additional four-fermion interactions in the effective model, arising from terms in the microscopic Hamiltonian, such as that of the Hubbard model of Ref. 16. Renormalization-group studies in the literature have so far not achieved consensus about whether such terms would be relevant[24] or not[25] at the graphene QCP.

Finally, while our model should be regarded as sharing universal features of graphene in the neighborhood of some putative fixed point and hence at best able to make predictions of critical exponents and dimensionless ratios of low-energy observables, it is difficult to resist the temptation to attempt to convert our result $g_c^{-2}(N_f=2)=0.609(2)$ for the critical coupling into a physical prediction.

First, we must express our result in terms of the continuum model (5). In order to do this, we remind the reader that the expression for the propagator [Eq. (6)] is derived using a regularization which respects current conservation; unfortunately the lattice regularization defined by Eq. (7) is not of this type. The solution, as outlined in Ref. 11, is to take the strong-coupling limit of the lattice model not at $g^{-2}=0$ but at $g^{-2}=g_{\rm lim}^{-2}$, which may be identified numerically via the location of a peak in $\langle\bar{\chi}\chi\rangle$.[12] The relation between the V propagator on the lattice and in the continuum is then[11]

$$D_{\rm latt}(p;g) = ZD_2'(p;g_R) = Z\left[\frac{1}{2g_R^2} + \frac{N_f}{8}\frac{|\vec{p}|^2}{(p^2)^{1/2}}\right]^{-1} \tag{22}$$

with $Z=(1-\frac{g^2}{g_{\rm lim}^2})^{-1}>1$ and $g_R^2=Zg^2$. The extra factor of 2 in the first term in square brackets results from a careful counting of the staggered fermion degrees of freedom in Eq. (7).

For our graphene model Fig. 1 of Ref. 10 suggests $g_{\rm lim}^{-2}=0.30(2)$, yielding a renormalized critical coupling $g_{cR}^2\simeq 3.26$. Now, in order to compare the quantum and classical terms in $D_{\rm latt}$ to define an effective value of λ, a momentum scale p is needed. Since the only length scale in the problem is the lattice spacing, a natural (if somewhat arbitrary) choice is $p_0=0$ and $|\vec{p}|=\frac{\pi}{2}$; this means that the propagators D_1 and $D_{\rm latt}$ match at a distance of roughly one lattice spacing. The matching condition $\lambda=g_R^2\pi/4$ yields $\lambda_c\approx 2.6$.

Since D_2 decays faster than D_1 at large distances, this estimate for λ_c is likely to be on the high side. We should however note two factors neglected in this simplified approach. First, the renormalization factor $Z\approx 2.0$ boosts the interaction strength of the lattice model; taking proper account of this will have the effect of raising the predicted λ_c. Second, the Fermi velocity v_F appearing in Eq. (2) and implicitly in Eq. (5) is the bare one, whereas presumably it is the renormalized $v_{FR}\approx 0.7v_F$ which has the experimental value 10^6 ms^{-1}. Since λ in Eq. (4) is defined in terms of the bare value, this correction has the effect of lowering the predicted λ_c, although it will also correct the λ values calculated for physically realized cases such as graphene which is either freely suspended or mounted on a substrate of known dielectric constant. In our view the uncertainty over the phenomenologically relevant value of v_F must ultimately be settled by an *ab initio* microscopic calculation; moreover, should it prove to be the case that $z<1$, then the very notion of a universal Fermi velocity becomes ill defined since $\lim_{p\to 0}\frac{dE}{dp}$ diverges.

Table II compares our estimate for the critical interaction strength with both that of the alternative simulation of Drut and Lähde,[7–9] with a value predicted using a

TABLE II. Predictions for the critical interaction strength for $N_f=2$ and for the critical number of flavors N_{fc} in the strong-coupling limit.

Reference	α_c	λ_c	N_{fc}
This work, Ref. 10		2.6	4.8(2)
7 and 9	1.11(6)	1.70(8)	4–6
25			2.03
4 and 5	2.33	3.66	2.55
26	1.13	1.77	3.6
27	1.16	1.82	3.5
28	1.62	2.54	2.8

renormalization-group treatment of radiatively induced four-fermion contact interactions,[25] and with one older and three more recent estimates[4,5,26–28] based on self-consistent diagrammatic calculations using model (2). Note that is conventional in the literature to quote the critical effective fine-structure constant $\alpha_c=4\lambda_c/\pi N_f$; here we show both parameters where appropriate. Also listed are estimates for the critical number of flavors N_{fc} corresponding to the location of the QCP in the strong-coupling limit. We argued in Ref. 10 that in this limit our model coincides with Eq. (2) and hence that $N_{fc}=4.8(2)$ is a robust nonperturbative prediction.

To give these numbers some meaning recall that λ is calculated to be 1.25 for graphene on a SiO_2 substrate, where experimentally it is known to be a conductor, and 3.4 in vacuum. Acknowledging the difficulties in obtaining precise numbers reviewed in the previous paragraphs, we may nonetheless observe that our simulations lend support to the mounting body of theoretical evidence that freely suspended graphene is an insulator.

ACKNOWLEDGMENTS

This project required approximately 1 000 000 core hours to complete. The CPUs used were either Intel(R) Xeon(R) E5420 or Dual-Core AMD Opteron(tm) 2218 in a dual configuration (2×2 cores). The authors wish to thank Diamond Light Source for kindly allowing them to use extensive computing resources and specifically Tina Friedrich, Frederik Ferner, and Alun Ashton for help in configuring and maintaining these resources. W.A. would like to thank Gwyndaf Evans for support and kind words of encouragement.

[1] K. S. Novoselov, A. K. Geim, S. V. Morozov, D. Jiang, M. I. Katsnelson, I. V. Grigorieva, S. V. Dubonos, and A. A. Firsov, Nature (London) **438**, 197 (2005).
[2] A. H. Castro Neto, F. Guinea, N. M. R. Peres, K. S. Novoselov, and A. K. Geim, Rev. Mod. Phys. **81**, 109 (2009).
[3] A. H. Castro Neto, Phys. **2**, 30 (2009).
[4] D. V. Khveshchenko, Phys. Rev. Lett. **87**, 246802 (2001).
[5] E. V. Gorbar, V. P. Gusynin, V. A. Miransky, and I. A. Shovkovy, Phys. Rev. B **66**, 045108 (2002).
[6] D. T. Son, Phys. Rev. B **75**, 235423 (2007).
[7] J. E. Drut and T. A. Lähde, Phys. Rev. Lett. **102**, 026802 (2009).
[8] J. E. Drut and T. A. Lähde, Phys. Rev. B **79**, 165425 (2009).
[9] J. E. Drut and T. A. Lähde, Phys. Rev. B **79**, 241405(R) (2009).
[10] S. J. Hands and C. G. Strouthos, Phys. Rev. B **78**, 165423 (2008).
[11] L. Del Debbio, S. J. Hands, and J. C. Mehegan, Nucl. Phys. B **502**, 269 (1997).
[12] S. Christofi, S. J. Hands, and C. G. Strouthos, Phys. Rev. D **75**, 101701(R) (2007).
[13] I. O. Thomas and S. J. Hands, Phys. Rev. B **75**, 134516 (2007).
[14] C. J. Burden and A. N. Burkitt, Europhys. Lett. **3**, 545 (1987).
[15] S. Duane, A. D. Kennedy, B. J. Pendleton, and D. Roweth, Phys. Lett. B **195**, 216 (1987).
[16] T. Paiva, R. T. Scalettar, W. Zheng, R. R. P. Singh, and J. Oitmaa, Phys. Rev. B **72**, 085123 (2005).
[17] I. F. Herbut, Phys. Rev. Lett. **97**, 146401 (2006).
[18] K. Binder and J.-S. Wang, J. Stat. Phys. **55**, 87 (1989).
[19] A. Kocić, J. B. Kogut, and K. C. Wang, Nucl. Phys. B **398**, 405 (1993).
[20] J. González, F. Guinea, and M. A. H. Vozmediano, Phys. Rev. B **59**, R2474 (1999); O. Vafek, Phys. Rev. Lett. **98**, 216401 (2007).
[21] S. A. Jafari, Eur. Phys. J. B **68**, 537 (2009).
[22] R. M. Hornreich, M. Luban, and S. Shtrikman, Phys. Rev. Lett. **35**, 1678 (1975).
[23] I. F. Herbut, Phys. Rev. Lett. **87**, 137004 (2001).
[24] M. S. Foster and I. L. Aleiner, Phys. Rev. B **77**, 195413 (2008); I. F. Herbut, V. Juričić, and O. Vafek, *ibid.* **80**, 075432 (2009).
[25] J. E. Drut and D. T. Son, Phys. Rev. B **77**, 075115 (2008).
[26] D. V. Khveshchenko, J. Phys.: Condens. Matter **21**, 075303 (2009).
[27] G. Z. Liu, W. Li, and G. Cheng, Phys. Rev. B **79**, 205429 (2009).
[28] O. V. Gamayun, E. V. Gorbar, and V. P. Gusynin, Phys. Rev. B **80**, 165429 (2009).